Water transport in gas diffusion layer of a polymer electrolyte fuel cell in the presence of a temperature gradient. Phase change effect

Benjamin Straubhaar, Joel Pauchet, Marc Prat

Water transport in gas diffusion layer of a polymer electrolyte fuel cell in the presence of a temperature gradient. Phase change effect

Benjamin Straubhaar [a,b], *Joel Pauchet* [c], *Marc Prat* [a,b,*]

[a] *INPT, UPS, IMFT (Institut de Mécanique des Fluides de Toulouse), Université de Toulouse, Allée Camille Soula, F-31400 Toulouse, France*

[b] *CNRS, IMFT, F-31400 Toulouse, France*

[c] *Fuel Cell Components Laboratory (LCPEM), LITEN, CEA, 17 rue des Martyrs, 38000 Grenoble, France*

ABSTRACT

The gas diffusion layer (GDL) is a crucial component as regards the water management in proton exchange membrane fuel cells. The present work aims at discussing the mechanisms of water transport in GDL on the cathode side using pore network simulations. Various transport scenarios are considered from pure diffusive transport in gaseous phase to transport in liquid phase with or without liquid–vapor phase change. A somewhat novel aspect lies in the consideration of condensation and evaporation processes in the presence of a temperature gradient across the GDL. The effect of thermal gradient was overlooked in previous works based on pore network simulations. The temperature gradient notably leads to the possibility of condensation because of the existence of colder zones within the GDL. An algorithm is described to simulate the condensation process on a pore network.

Introduction

The gas diffusion layer (GDL) in PEMFC has several functions, [1]. The GDL contributes to make more uniform the gas supply to the active layer. The GDL must also contribute to the water management by enabling the water in excess to leave the system on the cathode side without affecting too much the oxygen access to the active layer. A key question in this context is the nature of the water within the GDL, i.e. in gaseous phase or in liquid phase. Obviously, the transfer of the water in excess in vapor phase sounds the best option if the objective is to maintain all pores in the GDL accessible to oxygen. On the other hand, a GDL made hydrophobic generally leads to better performance. A possible effect of a hydrophobic agent makes sense only if water is present in liquid phase in the GDL. If the water transfer is in liquid phase, then as discussed in Ref. [2], it is indeed much better to make the GDL hydrophobic because this favors the formation of liquid capillary fingers occupying a small fraction of the pore space. The complementary fraction, free of water, is therefore available for the oxygen transport. Then it must be pointed out that a PEMFC typically operates at a temperature of about

* *Corresponding author*. INPT, UPS, IMFT (Institut de Mécanique des Fluides de Toulouse), Université de Toulouse, Allée Camille Soula, F-31400 Toulouse, France.

E-mail address: mprat@imft.fr (M. Prat).

80 °C, which corresponds to a relatively high vapor saturation pressure. Furthermore, as discussed for example in Ref. [3], a temperature difference is expected across the GDL with the highest temperature on the active layer side. Since the GDL is colder on the bipolar plate side, water condensation is likely and can be another mechanism leading to the occurrence of liquid water in the GDL [4,5]. Also, because of the temperature gradient or because the relative humidity in the bipolar plate channel can be lower than 100%, evaporation is also possible. In brief, several options are possible as regards the water transport across the GDL: 1) transport in vapor phase only, 2) transport in liquid phase only, 3) transport with liquid – vapor phase change.

In this context, the present work discusses different mechanisms of water transport in the gas diffusion layer (GDL) on the cathode side from a combination of simple estimate and two-dimensional pore network simulations in relation with the water management issue. The fuel cells motivating the study are classical PEMFC but the results could be of interest for the modeling of other categories of fuel cells, e.g. Ref. [6] for example.

Pore network simulations

The modeling of transport phenomena in porous media is generally performed within the framework of the continuum approach to porous media. This approach considers volume-average transport equations and relies on the concept of length scale separation, i.e. the averaging volume should be small compared to the size of the porous domain for the Darcy's scale equations to make sense. As discussed for instance in Ref. [7], a GDL is only a few pore sizes thick. This is an example of thin porous media [8] in which the length-scale separation criterion is not satisfied. Furthermore, as also discussed in Ref. [7], the scenario of slow liquid invasion in a hydrophobic porous medium leads to a regime called the capillary fingering regime, which is fractal and thus not compatible with the volume-averaged equations. The fact that the continuum approach is highly questionable is a strong argument in favor of an alternate approach. As in several previous works, e.g. Refs. [9–11], and references therein, we use a pore network approach. In the pore network approach, the pore space is represented by a network of pores interconnected by channels. The transport of interest is directly computed at the pore network scale outside the continuum framework. For simplicity, we consider a regular two-dimensional lattice as sketched in Fig. 1. The pores correspond to the nodes of the network. The interconnecting channels between two pores correspond to the constrictions or throats of the pore space. The pores are idealized as cubic bodies and the throats are ducts of square cross-section. The pore network is constructed by assigning pore body sizes from a Gaussian distribution in the range $[d_{tmin}, d_{tmax}]$ with d_{tmin} = 20 μm and d_{tmax} = 34 μm. The size of the porous domain isℓ x L where ℓ is the GDL thickness. As discussed in Ref. [7] representative values of L and ℓ are: L ~ 2 mm and ℓ ~ 300 μm. The lateral size L corresponds to a unit cell containing a rib and two half-channels of the bipolar plate. At the bipolar plate side, one part of the GDL is in contact with a solid phase, the rib, whereas the other part is in contact with the channel providing the oxygen. The lattice spacing (= the distance between two pores) is equal to 50 μm so that a 40 × 6 pore network in considered (40 is the number of pores in the lateral (in-plane) direction and 6 the number of pores across the GDL (thus in the through plane direction).

Water transfer in vapor phase

To discuss the nature of the water transfer within the GDL, we begin with some simple analytical computations. We assume that all the water produced in the active layer as a result of the electro–chemical reaction is directed toward the GDL on the cathode side. This is a conservative estimate since a fraction of the produced water should actually go toward the anode side. The production rate (in mol/s) is classically expressed as a function of the current density in the fuel cell as,

$$Q = \frac{iA}{2F} \tag{1}$$

where F is the Faraday's constant (F = 96485.34 C), i is the current density and A the cross-section surface area of the network ($A = 40 \times 50\ \mu m \times 50\ \mu m$ with our 2D approach).

Suppose the water transfer takes place in vapor phase by diffusion and consider for simplicity the gas as a binary mixture of oxygen and water vapor. An important parameter is then the relative humidity, denoted by RH, in the channel. The gas at the fuel cell inlet is not dry but humidified. Considering automotive applications, we can take for example $RH = 50\%$ at the inlet. As a result of water production, the relative humidity is expected to increase along the channel and can even be expected to reach almost 100% RH at the outlet of the fuel cell. Accordingly, we vary in what follows RH from about 50% to 100%. An additional simplification is to suppose that the gas is fully vapor saturated in humidity at the inlet of the GDL (the GDL inlet is the interface between the active layer and the GDL). Under these circumstances, the diffusive transport of the vapor can be expressed as,

$$J = \frac{cA}{\ell} D_{app}[\ln(1 - RH\, x_{vsat}(T_c)) - \ln(1 - x_{vsat}(T_{al}))] \tag{2}$$

with $c = p/RT$ where p is the total pressure (p ~ 1.5 bar), R is the gas constant, ℓ is as before the thickness of the GDL (~6 × 50 μm); $x_{vsat}(T_{al})$ is the vapor mole fraction at the active layer – GDL where T_{al} is the temperature at this interface; $x_v = RH\ x_{vsat}(T_c)$ at the GDL/channel interface where x_v is the mole fraction of vapor and T_c is the channel temperature.

In Eq. (2), D_{app} is the apparent diffusion coefficient of the GDL. It differs from the molecular diffusion coefficient because of the presence of the porous microstructure. Using the same method as reported for instance in Ref. [12], this coefficient is computed from pore network simulations taking into account that the GDL is partially blocked by the rib as depicted in Fig. 1. Repeating the simulations for 10 different realizations of network and ensemble-averaging the results led to $D_{app}/(\varepsilon D) = 0.19$ where D is the molecular diffusion coefficient of vapor ($D = 3.1\ 10^{-5}$ m^2/s at 80 °C) and $\varepsilon \approx 0.65$ is the network porosity. This enables us to define the critical current density i_c beyond which it is not possible to transfer all the

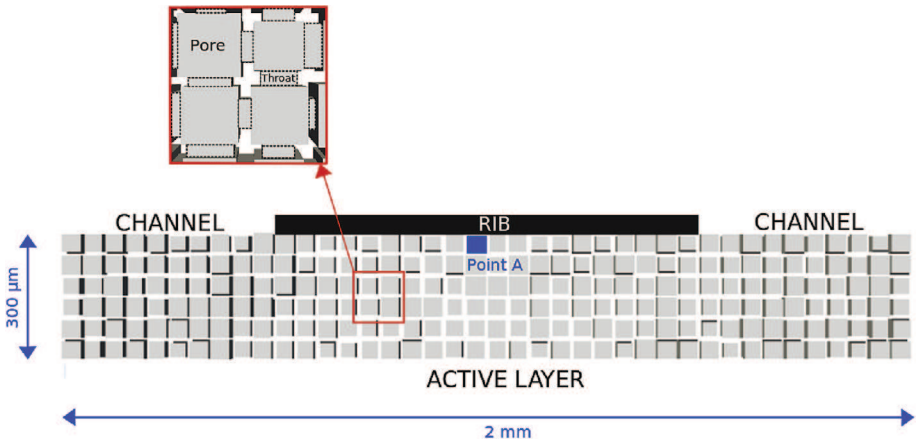

Fig. 1 – Sketch of GDL as a two-dimensional pore network.

produced water by diffusion in vapor phase through the GDL. This current is given by the equation $J = Q$. This yields,

$$i_c = \frac{2F\,c}{\ell} D_{app} \ln\left(\frac{1 - RH\, x_{vsat}(T_c)}{1 - x_{vsat}(T_{al})}\right) \quad (3)$$

The "critical" current i_c is plotted as a function of *RH* in Fig. 2 for the case $T_c = T_{al} = 80\ ^\circ C$.

As an example, the results plotted in Fig. 2 suggest that the produced water can be carried away in vapor phase as long as *RH* in the channel is lower than about 75% when $i = 1\ A/cm^2$. The conclusion of this section is therefore that at least two regions should be distinguished when analyzing the transport of water in the GDL in a fuel cell. In the region sufficiently away from the bipolar plate channel outlet for the relative humidity in the channel to be sufficiently low, the transfer could be in vapor phase only. Closer to the outlet, the transfer is not possible in vapor phase only and thus water should be present in liquid form, at least for sufficiently high current densities. Note, however, that the results shown in Fig. 2 were obtained assuming a uniform temperature across the GDL. As shown in Ref. [13] when a more accurate determination of critical current is presented, the existence of a temperature gradient changes the value of the critical current but not the main conclusion, i.e. the presence of liquid water when the relative humidity is sufficiently high in the channel.

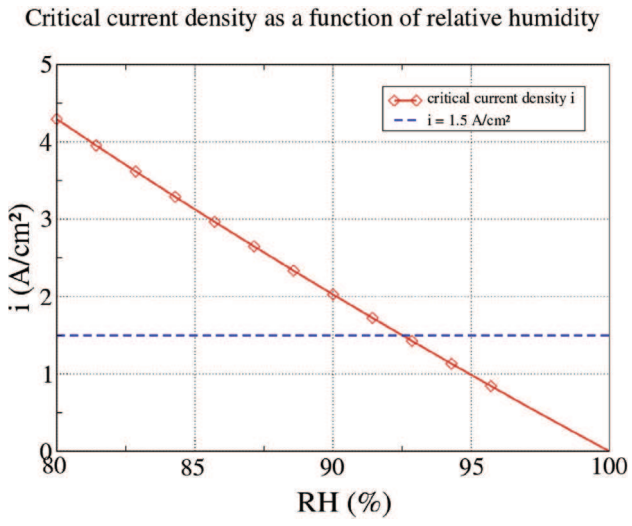

Fig. 2 – Critical current density i_c as a function of relative humidity RH in the channel.

Above the critical current, the produced water cannot be transferred only in vapor phase. This means that the GDL must be partially occupied by liquid water. Two main options are then possible depending on the boundary condition imposed at the active layer (AL) – GDL interface. The first option consists in assuming that water enters the GDL in liquid phase from the AL. By contrast, the second option is to consider that water enters the GDL in vapor phase from the AL. This second option can then lead to the formation of liquid water in the GDL only by condensation, i.e. when regions in the GDL are colder than the AL. The two options are discussed in what follows.

Transfer above the critical current density (negligible thermal gradient)

Transfer in liquid phase neglecting phase – change phenomena

Several authors have considered that water enters the GDL directly in liquid phase, e.g. Refs. [2,7,9–11,14,15], to cite only a few. Within the framework of pore network model, this scenario is simulated on a network using the classical invasion percolation (IP) algorithm [16]. Liquid water simulation with this algorithm consists of invading the network through a series of elementary invasion steps until the liquid reaches the channel. Each elementary step consists in invading the constriction (bond) of largest hydraulic diameter available along the liquid–gas interface as well as the gaseous pore adjacent to this constriction. This type of simulation typically leads to a capillary fingering invasion pattern as exemplified in Fig. 3. The 3D version of this pattern is qualitatively consistent with the experimental visualizations reported in Refs. [17], at least as regards the ramified structure of main liquid clusters.

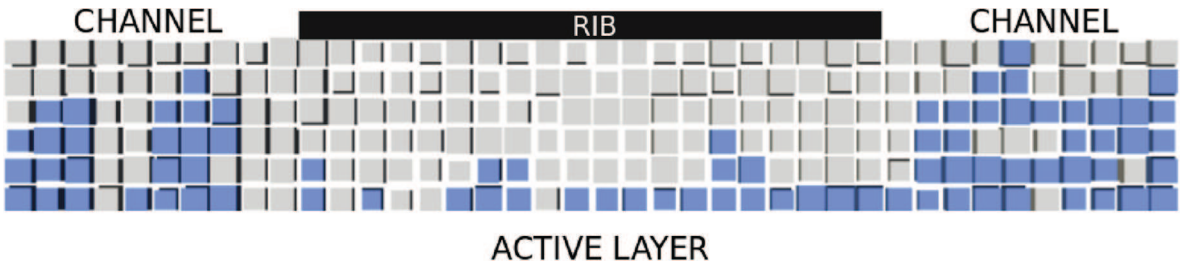

Fig. 3 – Two-dimensional typical slow invasion pattern in a hydrophobic layer from pore network simulation. Each square corresponds to a pore. Liquid phase in blue, gas phase in grey. (For interpretation of the references to color in this figure legend, the reader is referred to the web version of this article.)

As discussed in Refs. [9,18], one problem with this type of simulation lies in the boundary condition to be imposed at the inlet. It was argued in Ref. [18] that the consideration of independent multiple injection points at the GDL inlet was a better option that the traditional reservoir-like boundary condition. This, however, does not change the main feature of invasion pattern.

Transfer by evaporation with partial invasion of the GDL

In Section 5, we briefly consider the purely liquid invasion scenario ignoring the possible phase change phenomena. Since the vapor partial pressure at menisci along the boundary of the invading liquid cluster is the saturation vapor pressure then a transfer by vapor diffusion from these menisci toward the channel (supposed at a lower partial pressure in vapor) is possible.

This kind of situation can be easily simulated using a pore network model. The algorithm we developed for that purpose can be summarized as follows. Initially, the network is only occupied by the gas phase and the liquid/gas interface is supposed to coincide with the GDL/active layer interface. As for the other cases considered in this article, the medium is supposed to be fully hydrophobic so that the invasion percolation algorithm [16], can be used for modeling the liquid invasion on the network.

1) Let $i > i_c$. Determine the flow Q to be transferred from Eq. (1).
2) Determine the next throat to be invaded by the liquid using the classical invasion percolation algorithm [16]. Invade the corresponding throat and adjacent pore.
3) For the new position of the liquid–gas interface within the network, compute the molar flow J which is transferred by diffusion in vapor phase between the liquid/gas interface and the channel. Thus we impose $x_v = RH\ x_{vsat}(T)$ at the GDL/channel interface, a zero-flux condition at the GDL/rib interface and $x_v = x_{vsat}(T)$ on each meniscus which are in the system. This part of the algorithm is similar to the one presented in Ref. [12] for the calculation of the apparent diffusion coefficient D_{app}.
4) If $J < Q$ continue the invasion going back to 2). If $J \sim Q$, the steady-state solution with partial invasion is obtained.

An example of a result obtained with this algorithm is shown in Fig. 4.

We are not aware of in-situ visualizations, similar for example to the ones reported in Refs. [17], consistent with this scenario of partial liquid invasion with evaporation. It should be noted, however, that a special very small fuel cell was designed for making possible the visualizations reported in Ref. [17]. Thus, further investigations are needed to discuss the scenario illustrated in Fig. 4 from experiments.

Interestingly, a partial invasion of the GDL by the liquid water contributes to maintain a better access to oxygen compared to the situation, depicted in Fig. 3, where the evaporation phenomenon is not taken into account or is negligible (which can occur when the relative humidity in the channel is very high, close to 100% for example).

Transfer above the critical current density with consideration of thermal gradient

Until now, we have considered the temperature as uniform across the GDL. As mentioned before, authors, e.g. Ref. [3] for instance, have shown that a temperature difference ΔT of a few K occurs between the hotter active layer and the colder bipolar plate. Given the small thickness of the GDL (~300 μm) this represents a significant thermal gradient. This order of magnitude can be obtained from the following simple estimate. The electrochemical reaction is exothermic. The corresponding heat production per unit surface area (W m^{-2}) can be expressed as, e.g. Ref. [3],

$$\Phi = \left(\frac{h_{lv}}{2F} - U\right) i \tag{4}$$

where h_{lv} is the water latent heat of vaporization ($h_{lv} = 242{,}000$ J mol^{-1}), U the electrical tension.

It can be reasonably assumed that half of the produced heat goes toward the anode and half toward the cathode GDL. Using Fourier's law then leads to

$$0.5\,\Phi = 0.5\left(\frac{h_{lv}}{2F} - U\right) i = \lambda_{eff}\frac{T_{in} - T_{channel}}{H} \tag{5}$$

where λ_{eff} is the GDL effective thermal conductivity and H the thickness of the GDL. As representative value of the GDL thermal conductivity, we took $\lambda_{eff} = 1$ W m^{-1} K^{-1}. Application of Eq. (5) then leads to temperature differences across the GDL of a few K in qualitative accordance with the values reported in the literature. For a given temperature in the channel and

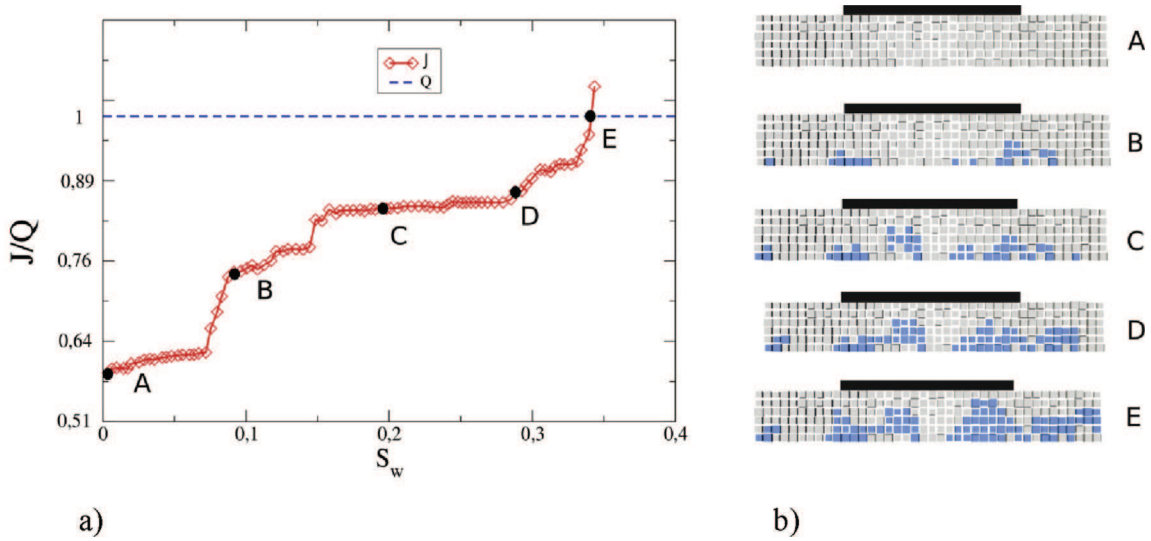

Fig. 4 – a) transferred water flux *J* for several invasion states of the GDL (T = 80 °C). S_w is the liquid saturation, b) invasion patterns corresponding to the points shown in Fig. 4a. The steady-state is reached (point E) when evaporation rate *J* is sufficient along the liquid–gas interface for transferring the produced water Q after partial invasion of network. Each little square corresponds to a pore. Liquid phase in blue, gas phase in grey. These results were obtained for *RH* = 96% (channel); *i* = 1.5 A/cm²; *ΔT* = 0 K (isothermal condition). (For interpretation of the references to color in this figure legend, the reader is referred to the web version of this article.)

given current density and electrical tension, Eq. (5) is used to determine T_{in} and then the temperature field in the GDL, which with the simplified approach considered in the present study is given by

$$T(x,y,z) = -\Delta T\frac{z}{H} + T_{in} \tag{6}$$

in which $\Delta T = T_{in} - T_{channel}$; x, and y are Cartesian coordinates in the in-plane direction and z in the through plane direction.

The first consequence of the temperature difference is that the transfer by vapor diffusion across the GDL is more efficient than for the uniform temperature situation with the same conditions in the channel because the equilibrium molar fraction x_{vsat} on the active layer/GDL interface increases with temperature. In other terms, the critical current plotted in Fig. 2 is underestimated when the temperature is not uniform and we consider that the vapor is saturated at the active layer – GDL interface, see Ref. [13] for more details.

The other important consequence of the temperature difference is the possible condensation of the vapor within the GDL because of the existence of the colder region on the channel side.

A first step in the study of the condensation process is to compute the vapor molar fraction field in presence of a thermal gradient in the domain shown in Fig. 1. Using again our pore network model, we impose the water production rate given by Eq. (1) at the active-layer/GDL interface, a given vapor molar fraction at the channel/GDL interface and zero flux condition at the rib/GDL interface. This computation is therefore similar to the one giving D_{app}. The result shows that the vapor molar fraction along the outlet of the GDL is located in the middle of the GDL – rib interface. This corresponds to point A in Fig. 1. The computation for realistic temperature differences shown that a condensation can indeed occur in the region of point A when the relative humidity is sufficiently high in the channel (the aforementioned computation leads to vapor molar fractions greater than the saturation vapor molar fraction at the corresponding temperature).

Interestingly, this is consistent with the experimental phase distributions reported in Ref. [17], which show the presence of a thin liquid layer all over the rib surface in contact with the GDL. Thus, under these conditions, a partial invasion in liquid phase of the GDL is expected from the growth of condensation clusters forming at the GDL/rib interface.

This situation can be simulated from pore network simulations using the following algorithm, which is presented in Ref. [13] in more details together with 3D simulations;

1) Determine and label the different water clusters present in the network. If two pores – totally or partially saturated in water – are adjacent, they belong to the same cluster. The first cluster at the very beginning is the pore in the network where the computed molar fraction is the highest above the saturation molar fraction.
2) Calculate the vapor molar fraction field x_v imposing the saturated molar fraction at the corresponding temperature along the boundary of each liquid cluster
3) Compute the molar flux F_k at the boundary of each cluster
4) Determine the throat of larger diameter along the boundary of each liquid cluster
5) Compute the invasion time t_k of each cluster *k*, i.e. the time required to fully invade the pore adjacent to the throat determined in #4 from F_k (step 3) and the volume remaining to invade in the considered pore.
6) Compute the time step $dt = \min(t_k)$.

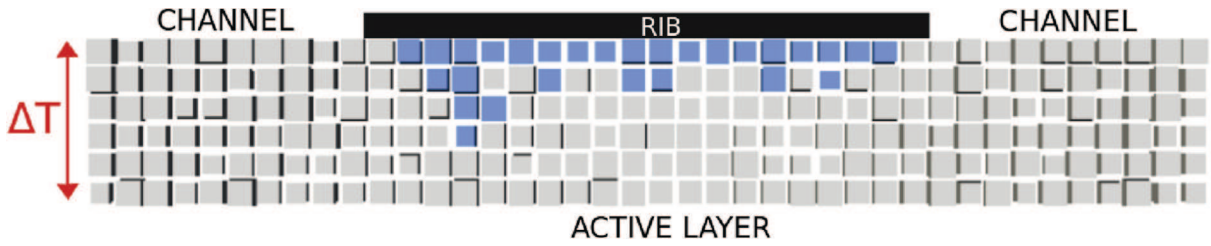

Fig. 5 – Partial liquid invasion of the GDL by condensation under the rib. Each little square corresponds to a pore. Liquid phase in blue, gas phase in grey. Pattern obtained for $RH = 97\%$ (channel); $i = 1.5$ A/cm^2; $\Delta T = 3.25$ K. (For interpretation of the references to color in this figure legend, the reader is referred to the web version of this article.)

7) Fully invade the pore corresponding to dt and update the volume of liquid in the invaded pore in the other clusters
8) Go back to step 1 until the water flux at the GDL outlet (GDL –channel interface) reaches a desired value, i.e. the water production rate given by Eq. (1).

Fig. 5 shows a typical phase distribution obtained with this algorithm for $T_{channel} = 80$ °C. As can be seen, this leads to an invasion pattern quite different from the ones depicted in Figs. 3 and 4. The liquid is moving forward, i.e. toward the bipolar plate, in the scenarios corresponding to Figs. 3 and 4 whereas it is rather moving on average toward the active layer in the condensation scenario.

Hence, the simulations illustrated in Fig. 5 do indicate a quite different liquid invasion scenario of GDL than considered in most previous pore network simulations.

As illlustrated in Figs. 6 and 7 the degree of liquid water invasion in the GDL due to condensation depends as expected on the curent density and the relative humidity in the channel. The greater the curent density for a given relative humidity RH in the channel, the greater the fraction of pores occupied by water in the GDL. Similarly, the greater the relative humidity RH for a given curent density, the greater the fraction of pores occupied by water in the GDL.

Discussion

Compared to most previous studies on water invasion of GDL by liquid water based on pore network simulations, the new feature introduced in the present article is the consideration of the liquid – vapor phase change process. In particular, the consideration of condensation leads to a quite different liquid invasion scenario of GDL than considered in most previous pore network simulations. It is therefore tempting to look at available experimental results in order to try to identify

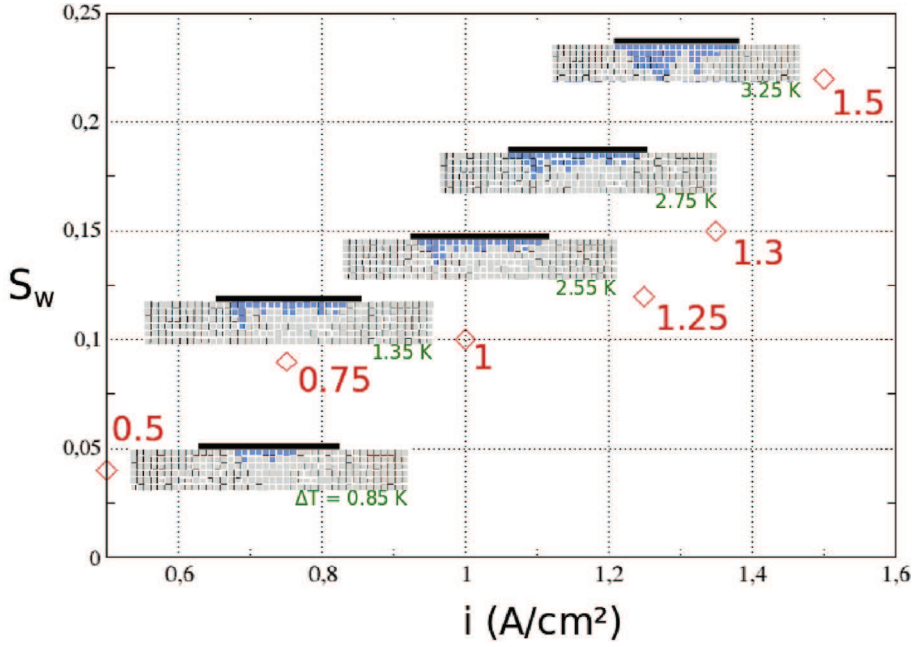

Fig. 6 – Variation of overall water saturation as a function of current density for $RH = 98\%$ together with corresponding condensation invasion patterns (shown for $i = 0.5$, 0.75, 1.25, 1.3 and 1.5 A/cm^2). Each little square corresponds to a pore. Liquid phase in blue, gas phase in grey. The temperature difference across the GDL corresponding to the imposed current density is indicated for each pattern shown. (For interpretation of the references to color in this figure legend, the reader is referred to the web version of this article.)

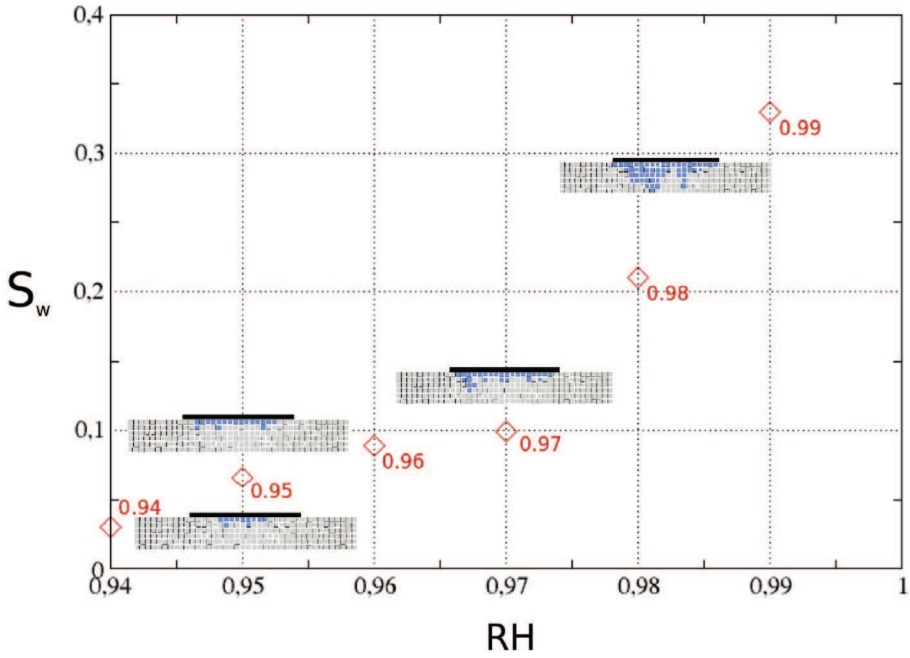

Fig. 7 – Variation of overall water saturation as a function of a channel relative humidity *RH* for $i = 1.5$ *A/cm²* together with corresponding condensation invasion patterns (for *RH* = 0.94, 0.95, 0.97 and 0.99 respectively). Each little square corresponds to a pore. Liquid phase in blue, gas phase in grey. $\Delta T = 3.25$ K. (For interpretation of the references to color in this figure legend, the reader is referred to the web version of this article.)

whether or not it is important to take into account condensation in the pore network simulations. A definitive conclusion is difficult to reach from the phase distributions obtained from X-ray tomography techniques [17]. The images of phase distribution reported in Ref. [17] present several features in favor of the condensation scenario. One can observe liquid clusters apparently disconnected from the AL/GDL interface and a massive presence of liquid under the ribs. However, one can also observe a droplet in the channel connected by a liquid cluster to the AL/GDL interface and is impossible to decide from the images whether the corresponding cluster is formed by condensation or by invasion in liquid phase from the AL. Also, we note that the visualizations reported in Ref. [17] were obtained for temperatures much lower (around 40 °C) than the temperature expected in an operating PEM (≈80 °C). A firm conclusion is also difficult to reach from the through plane saturation profiles reported in Ref. [19]. There are not in agreement with the pore network simulations considering only transport in liquid phase since the maximum in saturation can be in the middle of the GDL and not at the AL/GDL interface whereas the condensation simulations exemplified in Fig. 5 suggest a saturation maximum on the opposite side, that is to say on the channel – rib side. In brief none of the PN simulations performed so far led to a non-monotonous saturation profile with a maximum about in the middle of the GDL.

Actually, the condensation process is strongly dependent on the structure of the temperature field. Here, we are adopted a very simplified approach to compute this field, namely the analytical approach leading to Eq. (6). However, there are experimental evidences that the temperature is not uniform in the in-plane directions contrary to what we have assumed. The consideration of more representative temperature fields combined to 3D simulations is needed to go further in the comparison between experimental data and simulations. Naturally other aspects neglected in the present simulations such as the differential compression of the GDL under the rib and under the channel, the GDL anisotropy properties, the fact that the gas phase is a ternary mixture, etc, would need to be considered in a much more comprehensive approach.

The objective of the present paper was much more limited and was simply to discuss qualitatively various possible scenarios of water formation in GDL and for that we introduced the condensation algorithm. As mentioned before a much more extensive exploitation of this algorithm together with the consideration of more representative temperature fields will be presented in a forthcoming paper.

Conclusion

In addition to the classical purely capillarity controlled liquid invasion algorithm, two pore network models taking to account liquid – vapor phase change phenomena were described.

The results suggest that it could be important to distinguish different zones in the GDL along the channel of the bipolar plate on the cathode side in relation with the water management problem. Depending on the distance to the bipolar plate channel exit and for sufficiently high current densities, the different zones are as follows: a zone where the GDL is dry, a zone with partial liquid invasion and evaporation – condensation and finally a zone close to the exit of the channel with significant

liquid water invasion coming either directly in liquid phase from active layer or as a consequence of the evaporation – condensation process or both from the active layer in liquid phase and as a result of the condensation process.

The study also strongly suggests that liquid – vapor phase change phenomena are a crucial aspect in the analysis of water transfer in PEMFC. As a result of the phase change phenomena several mechanisms can contribute to the formation of liquid water in the GDL. Further studies are necessary to delineate more accurately the relative significance of each mechanism, namely capillary controlled liquid invasion, evaporation and condensation. This is important in relation with the design of GDL. This will be discussed in more details in a future work, notably from 3D pore network simulations.

Acknowledgments

The authors gratefully acknowledge the funding from the EU project IMPALA ("IMprove Pemfc with Advanced water management and gas diffusion Layers for Automotive application", project number: 303446) within the Fuel Cells and Hydrogen Joint Undertaking (FCHJU).

REFERENCES

[1] Barbir F. PEM fuel Cells: theory and practice. Elsevier Academic Press; 2005.
[2] Chapuis O, Prat M, Quintard M, Chane-Kane E, Guillot O, Mayer N. Two-phase flow and evaporation in model fibrous media. Application to the gas diffusion layer of PEM fuel cells. J Power Sources 2006;178:256–68.
[3] Thomas A, Maranzana G, Didierjean S, Dillet J, Lottin O. Thermal and water transfer in PEMFCs: investigating the role of the microporous layer. Int J Hydrogen Energy 2014;39(6):2649–58.
[4] Basu S, Wang CY, Chen KS. Phase change in a polymer electrolyte fuel cell. J Electroche Soc 2009;156(6):B748–56.
[5] Jiang FM, Wang CY. Numerical modeling of liquid water motion in a polymer electrolyte fuel cell. Int J Hydrogen Energy 2014;39:942–50.
[6] Celik C, Boyaci San FG, Sarac HI. Investigation of Ni foam effect for direct borohydride fuel cell. Fuel Cells 2012;12(6):1027–31.
[7] Rebai M, Prat M. Scale effect and two-phase flow in a thin hydrophobic porous layer. Application to water transport in gas diffusion layers of PEM fuel cells. J Power Sources 2009;192:534–43.
[8] Prat M, Agaësse T. Thin porous media, chapter 4. In: Vafai K, editor. Handbook of porous media-third edition. Taylor & Francis; 2015.
[9] Ceballos L, Prat M, Duru P. Slow invasion of a non-wetting fluid from multiple inlet sources in a thin porous layer. Phys Rev E 2011;84:056311.
[10] Ceballos L, Prat M. Slow invasion of a fluid from multiple inlet sources in a thin porous layer: influence of trapping and wettability. Phys Rev E 2013;87:043005.
[11] Gostick JT. Random pore network modeling of fibrous PEMFC gas diffusion media using Voronoi and Delaunay tessellations. J Electrochem Soc 2013;160(8):F731–43.
[12] Gostick JT, Ioannidis MA, Fowler MW, Pritzker MD. Pore network modelling of fibrous gas diffusion layers for polymer electrolyte membrane fuel cells. J Power Sources 2007;173:277–90.
[13] Straubhaar B, Pauchet J, Prat M. Pore network modelling of condensation in gas diffusion layers of proton exchange membrane fuel cells. [submitted 2015].
[14] Pasaogullari U, Wang CY. Liquid water transport in gas diffusion layer of polymer electrolyte fuel cell. J Electrochimic Soc 2004;151:A399–406.
[15] Nam JH, Kaviany M. Effective diffusivity and water-saturation distribution in single- and two layer PEMFC diffusion medium. Int J Heat Mass Transf 2003;46:4595–611.
[16] Wilkinson D, Willemsen JF. Invasion percolation: a new form of percolation theory. J Phys A Math Gen 1983;16:3365–76.
[17] Eller J, Rose T, Marone F, Stampanoni M, Wokaun A, Büchi FN. Progress in in situ x-ray tomographic microscopy of liquid water in gas diffusion layers of PEFC. J Electrochem Soc 2011;158(8):B963–70.
[18] Ceballos L, Prat M. Invasion percolation with multiple inlet injections and the water management problem in proton exchange membrane fuel cells. J Power Sources 2010;195:825–8.
[19] LaManna JM, Chakraborty S, Gagliardo JJ, Mench MM. Isolation of transport mechanisms in PEFCs using high resolution neutron imaging. Int J Hydrogen Energy 2014;39(7):3387–96.